RSC Advances

# LASER ABLATION OF A BULK CHROMIUM TARGET IN LIQUIDS FOR NANOPARTICLES SYNTHESIS



| | |
|---|---|
| Journal: | *RSC Advances* |
| Manuscript ID: | RA-COM-08-2014-008393.R1 |
| Article Type: | Communication |
| Date Submitted by the Author: | 11-Sep-2014 |
| Complete List of Authors: | Semaltianos, N.G.; AUTh, |
| | |



SCHOLARONE™
Manuscripts

# LASER ABLATION OF A BULK Cr TARGET IN LIQUIDS FOR NANOPARTICLES SYNTHESIS

N. G. Semaltianos*

University of Exeter

School of Physics

Exeter EX4 4QL

U.K.

## Abstract

Laser ablation of bulk target materials in liquids has been established as an alternative method for nanoparticles synthesis with unique and novel properties. Ablation of single element targets can lead to the synthesis of compound nanoparticles due to the interaction of the ablation plasma plume species with the species which are produced by the liquid decomposition. The additional compression which the plasma plume experiences by the liquid may result to the formation of nanoparticles which are characterized by metastable material phases, difficult or impossible to be produced by other methods. In this work laser ablation of a bulk Cr target in DI water, ethanol, acetone or toluene was carried out for the production of nanoparticles colloidal solutions. Mostly spherical nanoparticles are obtained in all four liquids with sizes ranging from 2 nm and up to a progressively smaller maximum diameter of 120, 50, 30 and 23 nm from DI water to toluene. Their size distribution follows log-normal function with a median diameter of 6.8, 11.2, 6.0 and 5.3 nm for the four liquids, respectively. Graphitic as well as amorphous carbon is found on the nanoparticles synthesized in the hydrocarbon liquids. The nanoparticles synthesized in DI water are a mixture of $Cr_3O_4$ and $Cr_2O_3$, in ethanol they are a mixture of $Cr_3O_4$, $Cr_7C_3$ and of the metastable phase $Cr_3C_{2-x}$ while in acetone or toluene nanoparticles of only of the metastable phase $Cr_3C_{2-x}$ are produced.

*Keywords:* nanoparticles; laser ablation; chromium carbide

*PACS:* 78.67.Bf - Nanocrystals and nanoparticles; 79.20.Eb - Laser ablation; 81.05.Je - Ceramics and refractories.

* Present address: Aristotle University of Thessaloniki, Department of Physics, Thessaloniki 54124, GREECE. E-mail: semal@auth.gr

**1. Introduction.**

Cr, the first of the group VI elements, is an important metal due mainly to its high corrosion resistance and hardness. It is mostly used as a surface wear and corrosion resistance coating by depositing it onto pre-treated metallic surfaces from suitable chemical precursors (hexavalent or trivalent Cr) using the technique of electroplating [1]. Of particular interest are the carbides of the metal because of their extreme hardness, corrosion resistance and refractory properties and especially $Cr_3C_2$ mainly because it has the greatest micro-hardness of all carbides [2]. Usually $Cr_3C_2$ crystals are added in the mixture of other metal carbides which are used in the manufacturing of cutting tools (such as tungsten carbide (WC)) and prevent the growth of large grains in the final composite upon sintering which in turn results in superior tool toughness [3]. $Cr_3C_2$ added to boron carbide ($B_4C$) during sintering results in an enhancement of its densification due to the formation of liquid phase [4]. The toughness and strength of alumina ($Al_2O_3$) is also enhanced by the addition of $Cr_3C_2$ particles [5].

$Cr_3C_2$ has a stable orthorhombic phase with space group Pbnm and it is usually synthesized by the arc melting (T>1400 ºC) of a mixture of pure Cr metal and graphite powder (the carbon source) under Ar gas atmosphere [6]. Another method involves the direct carburization of chromium oxide ($Cr_2O_3$) by methane ($CH_4$) or $CH_4$:Ar:$H_2$ gas mixture [7] or the reduction first of the oxide in Ar gas atmosphere using Al as a catalyst and then reaction of the pure Cr metal with graphite under ball mill mixing followed by heating at 800 ºC for 2 h [8]. With these methods chromium carbide in the form of irregular shape, micron-size particles is produced. Another method involves the reaction of a chemical precursor such as ammonium dichromate [$(NH_4)_2Cr_2O_7$] used as the chromium source with carbon black (the carbon source) in water, in which the mixture is first calcined at 180 ºC for 2 h following heating at high temperature (1100 ºC) for ~30 mins, which produces nanometer size particles (~30 nm) but with still irregular shapes [9].

The metastable phase of $Cr_3C_2$ with space group Cmcm is the disordered phase of the carbide and it can be formed either directly by the crystallization of C-rich amorphous $Cr_{1-y}C_y$ with $0.33 \leq y \leq 0.40$ alloys or for $0.40 \leq y \leq 0.52$ indirectly by the decomposition of the $CrC_{1-z}$ carbide at about 650 ºC which is also metastable and which is formed in a first step from the crystallization of the amorphous $Cr_{1-y}C_y$. It is symbolized as $Cr_3C_{2-x}$ ($0 \leq x \leq 0.5$) [10,11]. It has a filled-up Re3B-type structure in which the C atoms exists not only at prismatic but also at octahedral interstitial sites. This results to a departure from the $Cr_3C_2$ stoichiometry because of the partial occupation of the octahedral interstitial sites by C atoms. Octahedral interstitial sites are supposed to be unstable due to the energetically unfavourable electronic band structure. The fraction 1-x gives the fraction of occupied octahedral sites (or x of the empty sites).

Laser ablation of bulk target materials in liquids has been established as a method for the synthesis of nanoparticles in view of the advantages of the method that nanoparticle colloidal solutions with reduced reaction by-products are produced and nanoparticles with bare, ligand-free surfaces are synthesized since no chemical precursors are utilized in the synthesis as well as because the solutions are kept stable against nanoparticles agglomeration without the need of adding into them any stabilization surfactants [12]. Throughout the years, nanoparticles out of a number of different materials have been synthesized using this method. Usually laser ablation of a single metallic element target material in water leads to the formation of one or the different oxides of the metal while ablation in organic solvents leads to most of the times to the formation of carbides of the metal due to chemical reactions which take place between the ablation plasma plume species and the carbon species which are formed by the pyrolysis of the liquid. Thus laser ablation of a Ta target in ethanol lead to the synthesis of $Ta_xO$ crystal core/$Ta_2O_5$ amorphous shell nanoparticles [13]. Laser ablation of an Fe target in organic solvents lead to the synthesis of different oxide or carbide nanoparticles [14]. Similarly onion-like graphitized carbon-encapsulated $Co_3C$ core/shell nanoparticles were synthesised by laser ablation of a Co target in

acetone [15]. Laser ablation of a bulk Cr target in DI water was shown to produce predominantly spinel-type $Cr_3O_4$ nanoparticles with a small percentage of $\alpha$-$Cr_2O_3$ nanoparticles [16]. This communication involves the investigation of the laser ablation products of a bulk Cr target in DI water and in hydrocarbon liquid solvents such as ethanol, acetone and toluene.

**2. Experimental Details.**

Laser ablation for nanoparticles generation was carried out with a femtosecond (90 fs) pulsed laser at a beam wavelength of 800 nm and pulse repetition rate of 1 kHz using a pulse energy of 110 μJ. The target was a bulk piece of Cr metal (bcc) (purity 99.999%). Before ablation the target surface was mechanically polished using SiC paper in order to remove the thin protective (passivation) oxide surface layer which is typically formed onto the surface of Cr metal which is left standing in ambient air for sometime and then cleaned ultrasonically. The target was used for ablation immediately after polishing and ablation was carried out with the material lying at the bottom of a beaker filled with 5 ml of the liquid. The height of the liquid above the target surface was ~10 mm. The sample was moved under the stationary beam in a meander fashion (5 mm length, pitch 0.01 mm, scanning speed of 1 mm/s, 400 overscans) by using a computer controlled translational stage and ablation was carried out for ~35 mins each time. The nanoparticles colloidal solutions were stable against agglomeration for at least a month.

The nanoparticles colloidal solutions were characterized by UV-vis spectrophotometry (Jasco UV/vis/NIR V-570). The synthesized nanoparticles, from solution droplets dried out onto carbon coated copper grids, were characterized by Transmission Electron Microscopy (TEM) (JEOL JEM-2100 LeB6 200 kV) and from droplets dried out onto clean glass substrates by X-Ray Diffraction (XRD) using a diffractometer with a Cu $K_\alpha$ source ($\lambda$=1.5406 Å) (Bruker D8 Advance) and Raman spectroscopy (pumping beam at $\lambda$=514.48 nm, exposure time: 30 s,

excitation power: 50 %) (Renishaw InVia Microscope). Crystal structures were determined from the XRD spectra using the software of the instrument (DiffracPlus EVA)..

**3. Results and Discussion.**

Femtosecond laser irradiation of the Cr target under the present conditions of ablation using fluences of ~102 J/cm$^2$ results in the heating of the target surface at temperatures above the threshold for the material ablation to take place via the mechanism of phase explosion (6000 K) [17]. This has as a result the decomposition of the overheated material into a mixture of vapour and small liquid droplets. The nanoparticles are formed by nucleation of the ablation plume species in the vapour phase during the expansion and adiabatic cooling of the plasma plume within the liquid while a small number of nanoparticles (usually the larger ones) correspond to melted droplets which are ejected directly from the target surface.

XRD patterns measured from the nanoparticles are shown in Fig. 1. In the same graphs the reference patterns for the several material structures which are identified in the nanoparticles are also plotted for comparison. Although as it can be seen, the peaks in the patterns for the nanoparticles synthesized in ethanol, acetone or toluene are weak in intensity, however their intensities are sufficiently strong to allow for an unambiguous identification and assignment of the several peaks observed, to a particular crystal structure and to its corresponding reflections. Analysis of the patterns using the software of the diffractometer reveals that for the nanoparticles synthesized in DI water the patterns are matched to $Cr_3O_4$ and $Cr_2O_3$, in ethanol to $Cr_3O_4$, $Cr_7C_3$ and of the metastable phase $Cr_3C_{2-x}$ while in acetone or toluene to only of the metastable phase $Cr_3C_{2-x}$ [18]. $Cr_3C_2$ and $Cr_7C_3$ are two of the three thermodynamically stable carbides of chromium (the other one is $Cr_{23}C_6$) and their appearance in the synthesized nanoparticles is consistent with the fact that $Cr_3C_2$ has the lowest enthalpy of formation (-78 kJ/mol) before $Cr_7C_3$ (-143 kJ/mol) followed by $Cr_{23}C_6$ (-396 kJ/mol) [19] thus

it is more likely that in any reaction of chromium with carbon these carbides will be formed first as compared to other carbides.

TEM images of the nanoparticles are shown in Fig. 2 (a)-(d). It is seen that spherical nanoparticles are generated in DI water, ethanol and acetone while in toluene there are also a few nanoparticles which are not perfectly spherical. In case of DI water hollow nanoparticles are also formed. Such nanoparticles are typically formed in the case of laser ablation of different metals in water as a result of a preferential condensation and nucleation of the vaporized plume species at the interfaces between water and of the gas bubbles which are formed at the laser focal spot because of the ionization or evaporation of the water at the plume-water interface due to the extreme temperature of the plasma plume [20]. The size distribution histograms of the nanoparticles by counting approximately 400 nanoparticles in images of nanoparticles ensembles obtained on different areas on each grid, are shown in Fig. 2 (e)-(h). The histograms are described quire well by log-normal functions with median diameters of $<d_0>$=6.8, 11.2, 6.0 and 5.3 nm and standard deviations of $\sigma$=0.77, 0.67, 0.70 and 0.39, respectively. The narrower size distribution of the nanoparticles synthesized in the hydrocarbon liquids is attributed to the interaction of the ablation plume species with the carbon generated from the pyrolysis of the liquid by the extreme temperature of the plasma plume at the plume-liquid interface (this mechanism will be discussed later in the paper). The excess of carbon atoms which surrounds the embryonic nanoparticles interrupts their nucleation and hinders their growth [21]. The number of carbon atoms which are formed are expected to be larger as we go from ethanol to acetone to toluene due to the higher number of carbon atoms per molecule and this results in a successively smaller maximum nanoparticles diameter and narrower nanoparticles size distribution.

UV-vis absorption spectra measured from the nanoparticles colloidal solutions are shown in Fig. 3. The spectrum from the solution of the nanoparticles synthesized in DI water is

characterized by a broad band centred at ~382 nm and a weak peak at ~212 nm. The spectrum is similar to the one measured from the nanoparticles synthesized in DI water using long pulse laser ablation (240 μs, 1064 nm, 10 Hz, 1100 mJ) [16]. In particular, the high wavelength band which corresponds to a band gap energy of ~2.85 eV (estimated from the interception of the absorption onset with the horizontal axis from a plot of $(\alpha\omega)^2$ versus energy (inset in Fig. 3), assuming that the nanoparticles are crystalline direct band gap semiconductors [22] is attributed to $Cr^{2+}$ in $Cr_3O_4$ while the lower wavelength peak which corresponds to a band gap energy of ~4.8 eV is attributed to the spin allowed d-d transition of $Cr^{3+}$ ions ($3d^3$) in $Cr_2O_3$ in agreement with the band gap energy of bulk $Cr_2O_3$ [23]. Similar analysis applied for the spectra for the nanoparticles synthesized in acetone or toluene tends to be inconclusive due to the total opaqueness of the solvents at wavelengths below ~330 nm and ~280 nm, respectively, thus it is omitted here.

Raman spectra from the nanoparticles are shown in Fig. 4. The disorder D-band at ~1370 $cm^{-1}$ which is a breathing mode with $A_{1g}$ symmetry known to be due to the crystalline disorder and structural defects of graphite and of the graphitic G-band at ~1580 $cm^{-1}$ known to correspond to the $E_{2g}$ mode (stretching vibrations of $sp^2$ aromatic rings) in the basal plane of graphite [24] are easily resolved in the spectra from the nanoparticles synthesized in the hydrocarbon liquids. The G-band is narrower in width and stronger in intensity than the D-band. These indicate the presence of graphitic carbon in the nanoparticles (with the same chemical structure as graphite) while the relatively wide D-band indicates the presence of amorphous carbon resulting from disordered carbon layers or amorphous hydrogenated carbon resulting from the incorporation of hydrogen or oxygen atoms into the graphite layer [25]. These confirm once again the presence of carbon atoms during ablation (as well as of hydrogen ions and/or atoms), produced by the pyrolysis of the hydrocarbon liquid due to the extreme temperature of the ablation plasma plume or photolysis of the liquid by the laser beam, which

reacts with the chromium plume species leading to the production of chromium carbides in addition to carbon-based hydrogen or oxygen radicals. Spectra from the nanoparticles synthesized in DI water in the low wavenumbers region (200-650 $cm^{-1}$) (Fig. 4(b)) show a strong Raman band at 551 $cm^{-1}$ (d) which is assigned to $A_{1g}(2)$ optical mode and weak bands at 307 (a), 350 (b), 530 (c) and 609 $cm^{-1}$ (e) for Cr ions in octahedral sites, which are assigned to $E_g(2)$, $E_g(3)$, $E_g(4)$ and $E_g(5)$ modes, respectively. All these bands are due to $Cr_2O_3$ [26]. Careful observation of the spectra reveals that a weak band at 541, 542 and 548 $cm^{-1}$ is also present in the spectra from the nanoparticles synthesized in ethanol, acetone or toluene, respectively. Although this band is observed at wavenumbers very close to the position of the d band of the nanoparticles synthesized in DI water, the difference in lineshape indicates structural differences. This band is attributed to α-CrO(OH) (chromium oxyhydroxide) ($\nu_3$ $Cr^{III}$-O anti-symmetric stretching vibration) [27,28]. Raman bands from this compound are expected to be observed at similar wavenumber range as from $Cr_2O_3$ due to the presence of $[Cr^{III}O_6]$ octahedra in both compounds. a-CrO(OH) is observed as a corrosion product of Cr which was heated at 374 ºC under air saturated water at pressures of 25 MPa [27]. Peaks from this compound are not observed in the XRD patterns which indicates that its content in the synthesized nanoparticles ensemble is extermely low, estimated to be less than 1 % thus it is considered as a trace impurity.

In the cases of all four liquids, formation of the oxide or carbide nanoparticles is due to chemical reactions which take place between the ablation plasma plume species (ions, atoms or clusters of Cr) and the species which originate mainly from the thermal decomposition of the liquid at the plasma plume-liquid interface due to the extreme temperature of the plasma plume. A percentage of carbon or oxygen ions is also produced by the photolysis of the hydrocarbon liquid solvent by the laser beam [29,30,31]. In the case of DI water thermolysis leads to the generation of hydrogen and oxygen atoms and ions as well as hydroxyl ions [32].

The oxygen species react with the chromium species in the plasma plume and cause their oxidation and conversion to chromium oxides ($Cr_3O_4/Cr_2O_3$). In the case of the hydrocarbon liquids the thermochemical reactions cause the pyrolysis of the liquid which has as a result the formation of carbon ions or atoms either directly or via the decomposition of a variety of hydrocarbon or oxyhydrocarbon intermediate products [33-38]. These carbon species are first formed at the plume-liquid interface as well as within the laser beam path and as the plume expands adiabatically within the liquid, under the liquid compression they diffuse into the plume volume and mix with the chromium plume species. Decomposition of the liquid molecules and/or of the intermediate oxyhydrocarbon products also leads to the formation of oxygen ions or radicals which also diffuse within the plume volume and react with the plume species. In the case of toluene the oxygen ions or radicals originate from the atmospheric oxygen which exists dissolved in the liquid. This explains the presence of a very small percentage of chromium oxyhydroxide in the synthesized nanoparticles. The most probable reaction path involves the formation of metastable $CrO_2$ in a first step and its subsequent reduction by hydroxyl ions ($OH^-$) which are also formed as a result of the liquid decomposition. Under the widely varied pressure, temperature and density conditions of the plasma plume the carbon species interact with the chromium plasma species and the reactants are taken within a region of the equilibrium phase diagram in which metastable chromium carbide phases exist. When later the plume expansion quenches the metastable chromium carbide phase is "frozen" in the generated nanoparticles.

**4. Conclusions.**

This work demonstrates the possibility of synthesizing chromium oxide or chromium carbide nanoparticles or a mixture of them by laser ablating a bulk Cr target in liquid. Synthesis of oxide or carbide nanoparticles for a given set of laser ablation parameters, is determined by

the type of the liquid in which ablation takes place. $Cr_3C_2$ and particular its metastable phase $Cr_3C_{2-x}$ is an important ceramic compound and industrial material due to its extreme hardness, corrosion resistance and refractory metal properties. When chromium carbide particles are integrated into the surface of a metal it improves the wear and corrosion resistance of the metal and maintains these properties at elevated temperatures. Usually the particles are deposited onto the metal surface by spray deposition after dissolving the dry powder in a suitable liquid solvent such as acetone [39]. Fabrication of chromium carbide nanoparticles colloidal solutions at the present work by using the method of laser ablation of the bulk target material in liquid solvent provides with the advantage of a direct one-step process of formation of the solution which is to be deposited since the nanoparticles are synthesized directly into the liquid solvent by laser ablating the bulk target material in the solvent. Also nanometer size particles which are produced at the present work are likely to provide with a more uniform coating of the particular metal part surface as compared to the micron size particles. In addition, the bare surfaces of the nanoparticles provide with a superior quality of the interface between the nanoparticles and the underlying substrate. As it is well known, nanoparticles synthesized using laser ablation of metallic targets in liquids are usually electrically charged due to the partial oxidation of their surfaces induced by the reactive laser plasma [40,41] which is also the reason for the observed stability of the nanoparticles colloidal solutions against agglomeration without the need of adding to the solution any stabilizing ligands. Thus furthermore and most importantly chromium carbide nanoparticles colloidal solutions synthesized by laser ablation may allow the deposition of the nanoparticles onto any shape surface in an easy process using the method of electrophoretic deposition which is applied in industrial processes [42]. This emphasizes the importance of the method of synthesizing $Cr_3C_{2-x}$ nanoparticles by laser ablation of the bulk Cr target material in liquids presented in this work.

**Aknowledgements**

NGS aknowledges Prof. E. Hendry for providing access to his laser facilities and Dr. H. Chang and Dr. L. Wears for TEM and XRD measurements.

**References**

[1] D. J. Barclay and W. M. Morgan, USA Patent, US 4161432 A, July 17, (1979).

[2] S. Sharafi and S. Gomani, Int. J. Refract. Met. & Hard Mater., 30, 57 (2012).

[3] P. Schwarzkopf, R. Kieffer, W. Leszynski and F. Benesovsky, "Refractory hard metals: borides, carbides, nitrides and silicides", Macmillan, New York, (1953).

[4] X. Li, D. Jiang, J. Zhang, Q. Lin, Z. Chen and Z. Huang, J. Europ. Cer. Socie., 34, 1073 (2014).

[5] F. C. -Tsu and L. A. -Kang, Mater. Chem. Phys., 39, 129 (1994).

[6] S. Rundqvist and G. Runnsjö, Act. Chem. Scand., 23, 1191 (1969).

[7] N. Anacleto and O. Ostrovski, Met. Mater. Trans. B, 35, 609 (2004).

[8] O. M. Cintho, E. A. P. Favilla, J. D. T. Capocchi, J. All. Comp., 439, 189 (2007).

[9] Z. Zhao, H. Zheng, Y. Wang, S. Mao, J. Niu, Y. Chen and M. Shang, Int. J. Ref. Met. & Hard Mater., 29, 614 (2011).

[10] E. Bouzy, E. B. -Grose and G. Le Caër, Phil. Mag. B, 68, 619 (1993).

[11] E. Bouzy, G. Le Caër and E. Bauer-Grosse, Mat. Scie. Eng. A, 133, 640 (1991).

[12] G. W. Yang, Prog. Mater. Scie., 52, 648 (2007).

[13] Q. Li, C. Liang, Z. Tian, J. Zhang, H. Zhang and W. Cai, CrystEngComm, 14, 3236 (2012).

[14] V. Amendola, P. Riello and M. Meneghetti, J. Phys. Chem. C, 115, 5140 (2011).

[15] H. Zhang, C. Liang, J. Liu, Z. Tian and G. Shao, Carbon, 55, 108 (2013).

[16] C. H. Lin, S. Y. Chen and P. Shen, J. Phys. Chem. C, 113, 16356 (2009).

[17] E. T. Karim, Z. Lin and L. V. Zhigilei, AIP Conference Proceedings, 1464, 280 (2012).

[18] JCPDS No. 00-012-0559 ($Cr_3O_4$), JCPDS No. 00-002-1362 ($Cr_2O_3$), JCPDS No. 00-011-0550 ($Cr_7C_3$), JCPDS No. 03-065-0897 ($Cr_3C_{2-x}$).

[19] C. Jiang, Appl. Phys. Lett., 92, 041909 (2008).

[20] Z. Yan, R. Bao and D. B. Chrisey, Nanotechn., 21, 145609 (2010).

[21] V. Amendola, G. A. Rizzi, S. Polizzi and M. Meneghetti, J. Phys. Chem. B, 109, 23125 (2005).

[22] S. Hong, E. Kim, D. -W. Kim, T. -H. Sung and K. No, J. Non-Crystal. Solids, 221, 245 (1997).

[23] G. V. Samsonov, "The Oxide Handbook", IFI/Plenum, New York, 1982.

[24] F. Tuinstra and J. L. Koenig, J. Chem. Phys., 53, 1126 (1970).

[25] M. Veres, M. Füle, S. Tóth, M. Koós and I. Pócsik, Diam. Relat. Mater., 13, 1412 (2004).

[26] I. R. Beattie and T. R. Gilson, J. Chem. Soc. A, 980 (1970).

[27] J. E. Maslar, W. S. Hurst, W. J. Bowers Jr, J. H. Hendricks, M. I. Aquino and I. Levin, Appl. Surf. Scie., 180, 102 (2001).

[28] J. Yang, W. N. Martens and R. L. Frost, J. Raman Spectr., 42, 1142 (2011).

[29] A. Hu, J. Sanderson, A. A. Zaidi, C. Wang, T. Zhang, Y. Zhou and W. W. Duley, Carbon, 46, 1792 (2008).

[30] J. Chen, R. Ma, H. Ren, X. Li, H. Yang and Q. Gong, Int. J. Mass Spectr., 241, 25 (2005).

[31] A. D. Tasker, L. Robson, K. W. D. Ledingham, T. McCanny, S. M. Hankin, P. McKenna, C. Kosmidis, D. A. Jaroszynski and D. R. Jones, J. Phys. Chem. A, 106, 4005 (2002).

[32] S. Z. Baykara, Int. J. Hydr. Energy, 29, 1459 (2004).

[33] J. Li, A. Kazakov and F. L. Dryer, J. Phys. Chem. A, 108, 7671 (2004).

[34] S. Yang, W. Cai, H. Zeng and X. Xu, J. Mater. Chem., 19, 7119 (2009).

[35] D. J. Bradley, M. H. R. Hutchinson and H. Koetser, Proc. Roy. Soc. A, 329, 105 (1972).

[36] S. H. Mousavipour and P. D. Pacey, J. Phys. Chem., 100, 3573 (1996).

[37] J. R. McNesby, T. W. Davis and A. S. Gordon , J. Chem. Phys., 21, 956 (1953).

[38] M. B. Colket and D. J. Seery, 25th Symp. Intern. on Combustion, 25, 883 (1994).

[39] C. Tassin, F. Laroudie, M. Pons and L. Lelait, Surf. Coat. Techn., 80, 207 (1996).

[40] M. Shoji, K. Miyajima and F. Mafuné, J. Phys. Chem. C, 112, 1929 (2008).

[41] W. Guo and B. Liu, ACS Appl. Mater. Interf., 4, 7036 (2012).

[42] L. Besra and M. Liu, Prog. Mater. Scie., 52, 1 (2007).

**FIGURE CAPTIONS**

FIG. 1. XRD patterns of the nanoparticles.

FIG. 2. TEM images and corresponding size distribution histograms of the nanoparticles synthesized in: DI water (a and e), ethanol (b and f), acetone (c and g), and toluene (d and h), respectively.

FIG. 3. UV-vis absorption spectra measured from the nanoparticles colloidal solutions. Inset shows $(\alpha\omega)^2$ versus energy.

FIG. 4. Raman spectra of the nanoparticles.

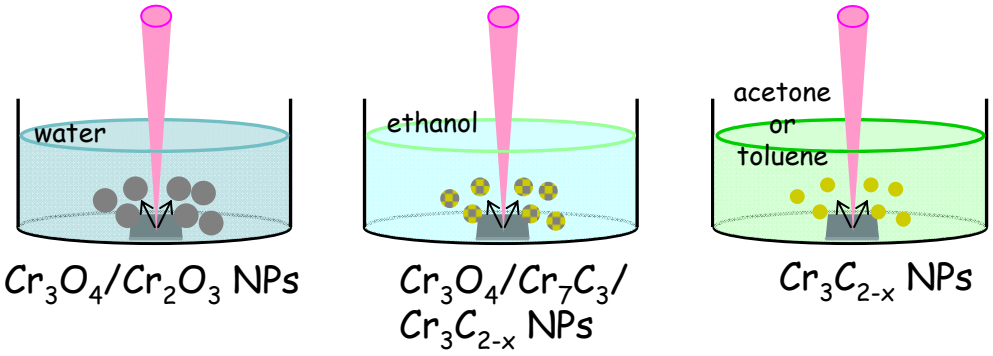
water
ethanol
acetone
or
toluene
$Cr_3O_4/Cr_2O_3$ NPs
$Cr_3O_4/Cr_7C_3/$
$Cr_3C_{2-x}$ NPs
$Cr_3C_{2-x}$ NPs

Chromium carbide nanoparticles in the metastable phase are synthesized by laser ablation of a bulk chromium target in acetone or toluene

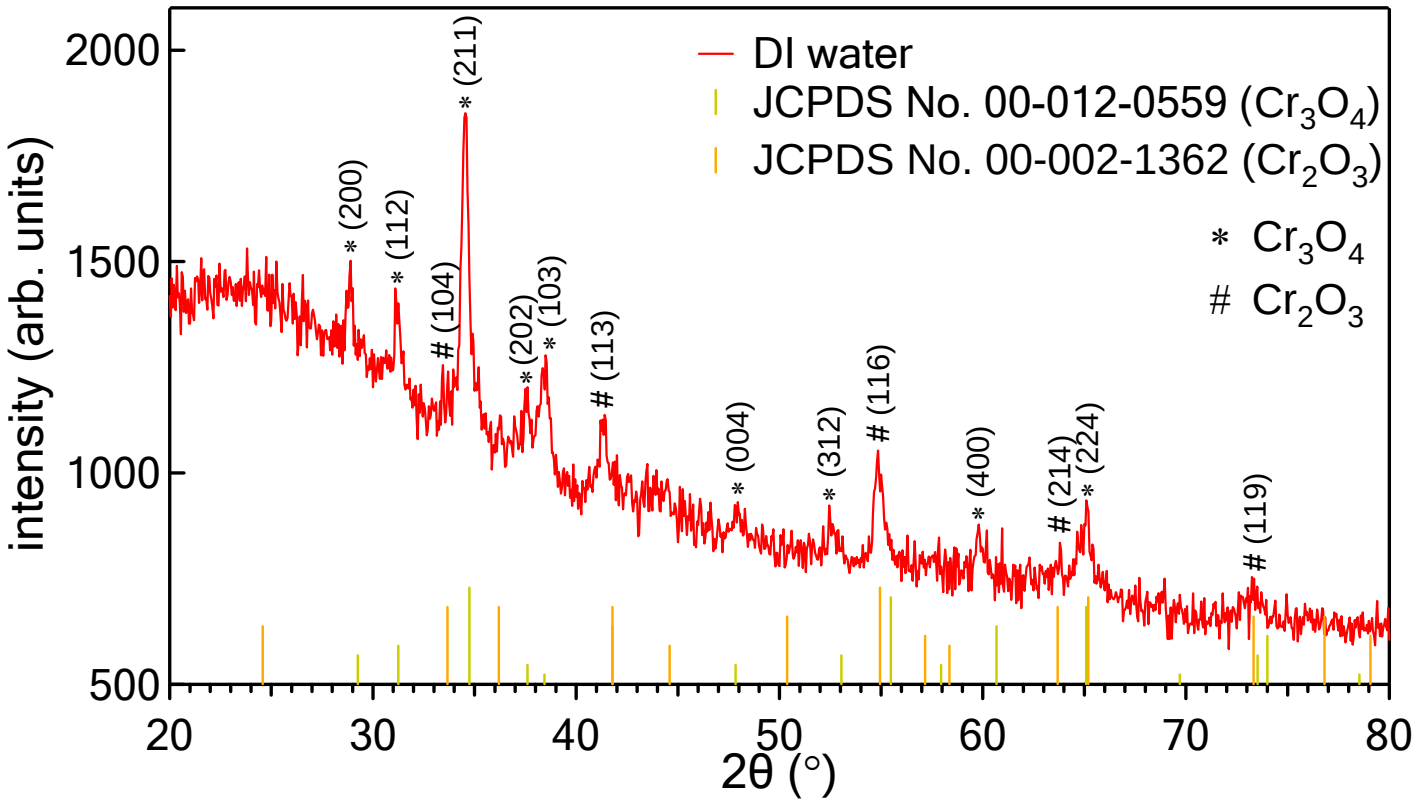
DI water
JCPDS No. 00-012-0559 ($Cr_3O_4$)
JCPDS No. 00-002-1362 ($Cr_2O_3$)
* $Cr_3O_4$
# $Cr_2O_3$
* (200)
* (112)
# (104)
* (211)
*(202)
* (103)
# (113)
* (004)
* (312)
# (116)
* (400)
# (214)
* (224)
# (119)
intensity (arb. units)
2θ (°)
2000
1500
1000
500
20
30
40
50
60
70
80

Fig. 1(a)

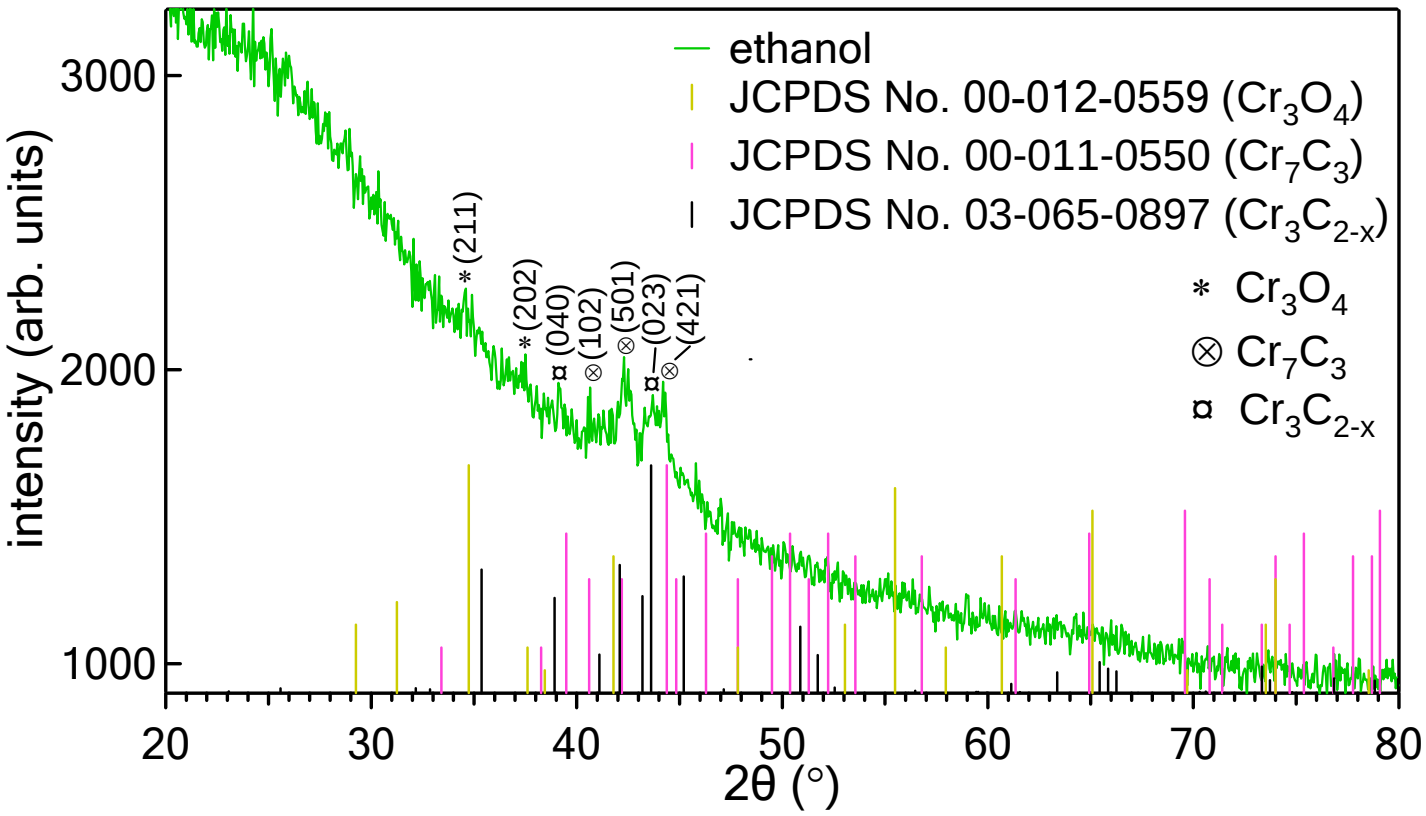
ethanol
JCPDS No. 00-012-0559 ($Cr_3O_4$)
JCPDS No. 00-011-0550 ($Cr_7C_3$)
JCPDS No. 03-065-0897 ($Cr_3C_{2-x}$)
* $Cr_3O_4$
⊗ $Cr_7C_3$
¤ $Cr_3C_{2-x}$
* (211)
* (202)
¤ (040)
⊗ (102)
⊗ (501)
¤ (023)
⊗ (421)
intensity (arb. units)
3000
2000
1000
20
30
40
50
60
70
80
2θ (°)

Fig. 1(b)

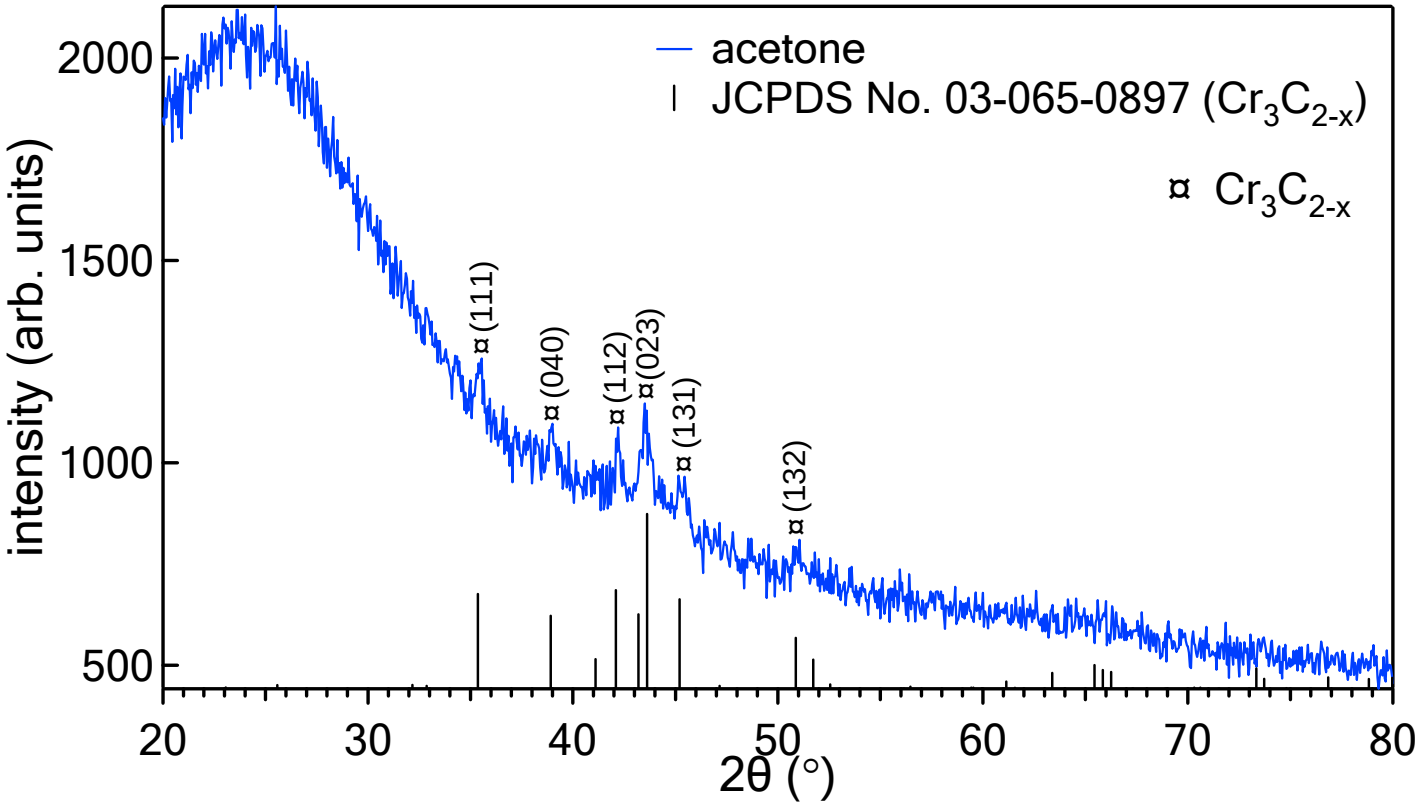
acetone
JCPDS No. 03-065-0897 ($Cr_3C_{2-x}$)
¤ $Cr_3C_{2-x}$
¤(111)
¤(040)
¤(112)
¤(023)
¤(131)
¤(132)
intensity (arb. units)
2θ (°)
2000
1500
1000
500
20
30
40
50
60
70
80

Fig. 1(c)

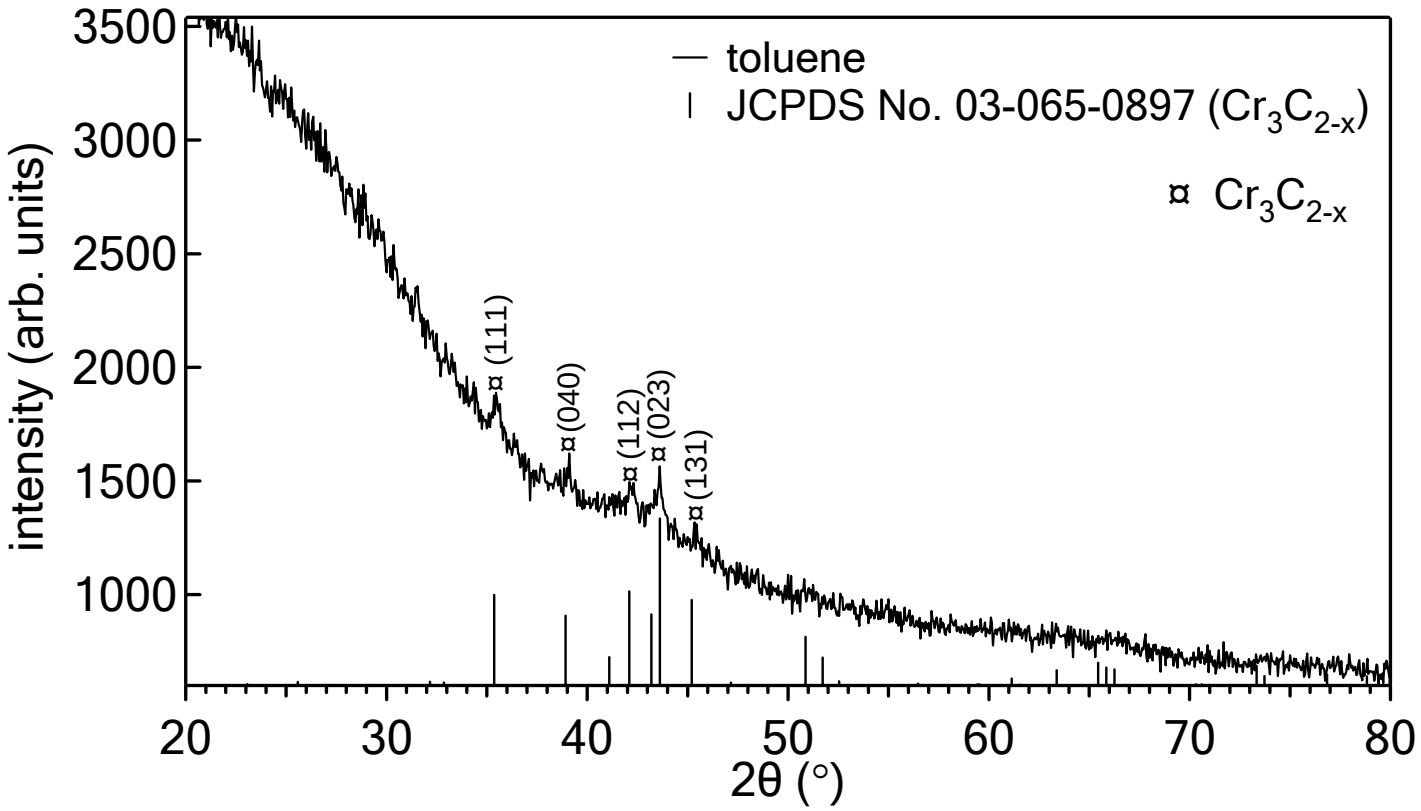
toluene
JCPDS No. 03-065-0897 ($Cr_3C_{2-x}$)
¤ $Cr_3C_{2-x}$
¤ (111)
¤ (040)
¤ (112)
¤ (023)
¤ (131)
intensity (arb. units)
2θ (°)
3500
3000
2500
2000
1500
1000
20
30
40
50
60
70
80

Fig. 1(d)

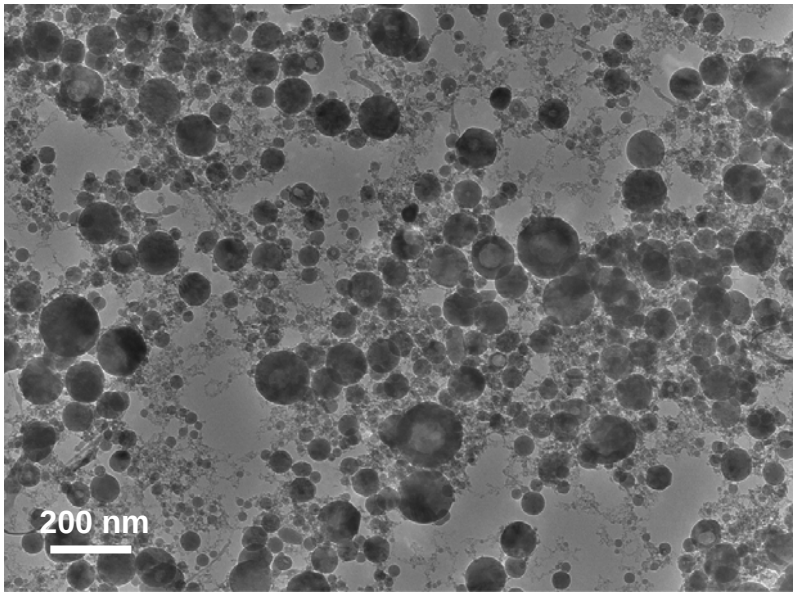
200 nm

(a)

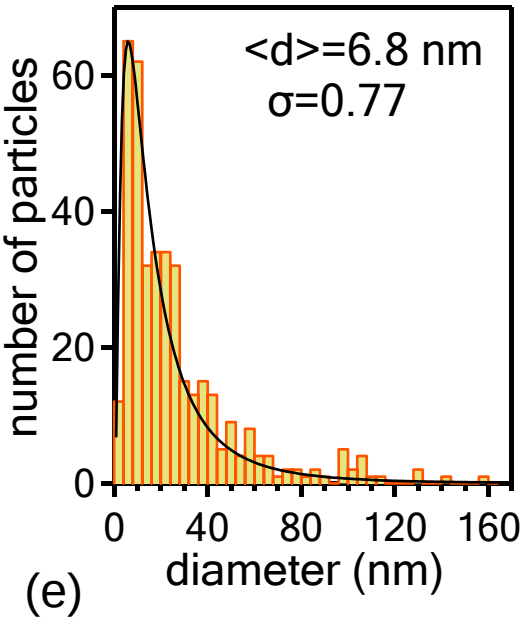
<d>=6.8 nm
σ=0.77
number of particles
0
20
40
60
0
40
80
120
160
diameter (nm)

(e)

Fig. 2(a),(e)

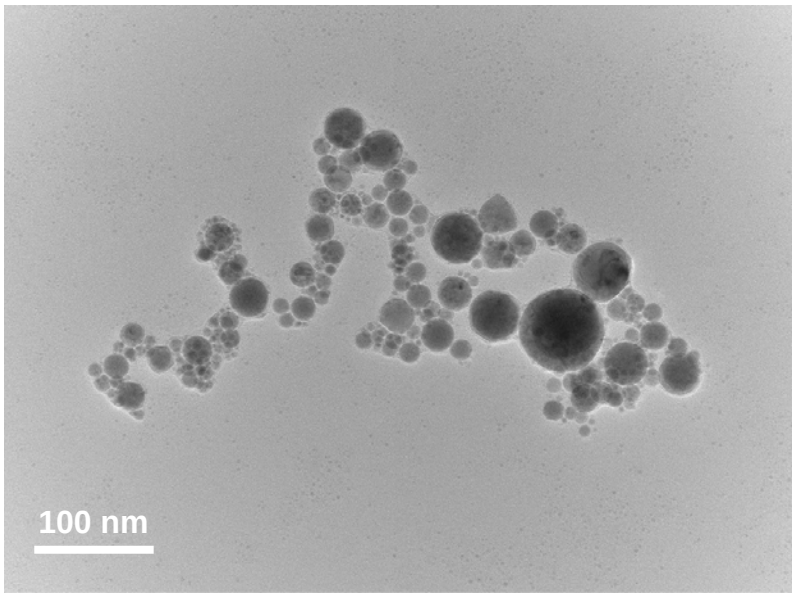
100 nm

(b)

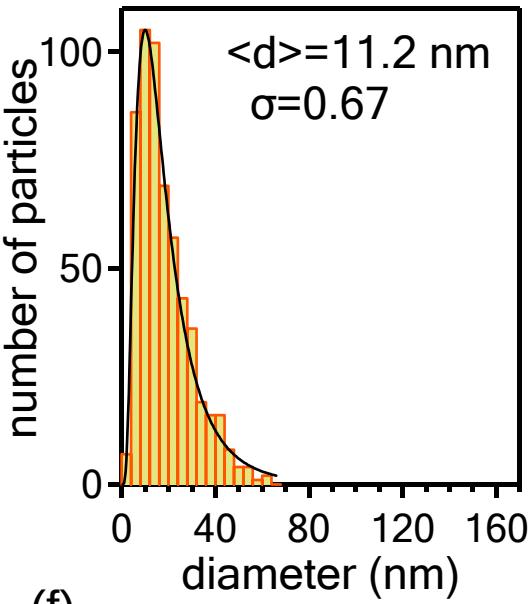
<d>=11.2 nm
σ=0.67
number of particles
100
50
0
0
40
80
120
160
diameter (nm)

(f)

Fig. 2(b),(f)

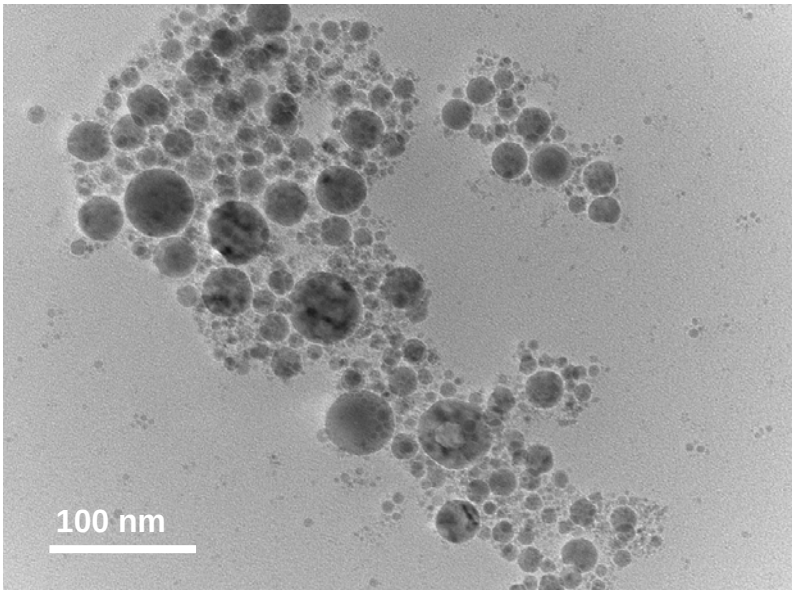
100 nm

(c)

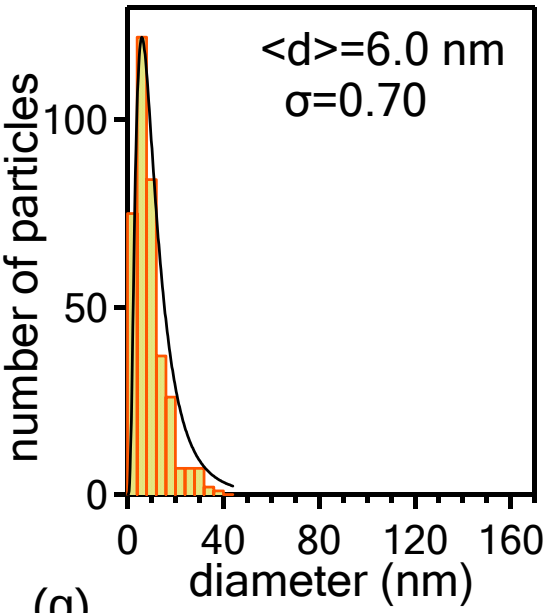
<d>=6.0 nm
σ=0.70
number of particles
100
50
0
0
40
80
120
160
diameter (nm)

(g)

Fig. 2(c),(g)

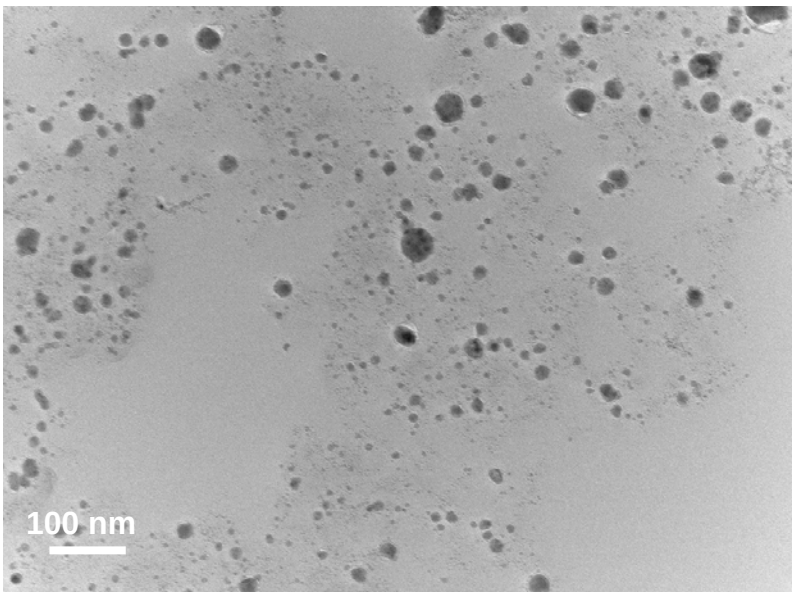
100 nm

(d)

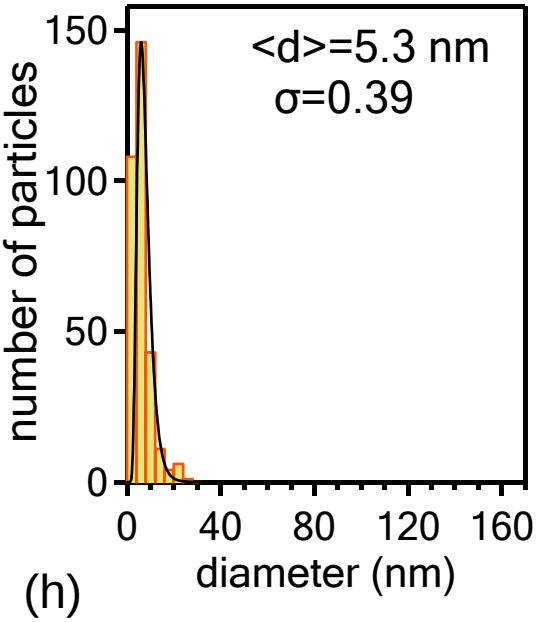
<d>=5.3 nm
σ=0.39
number of particles
150
100
50
0
0
40
80
120
160
diameter (nm)

(h)

Fig. 2(d),(h)

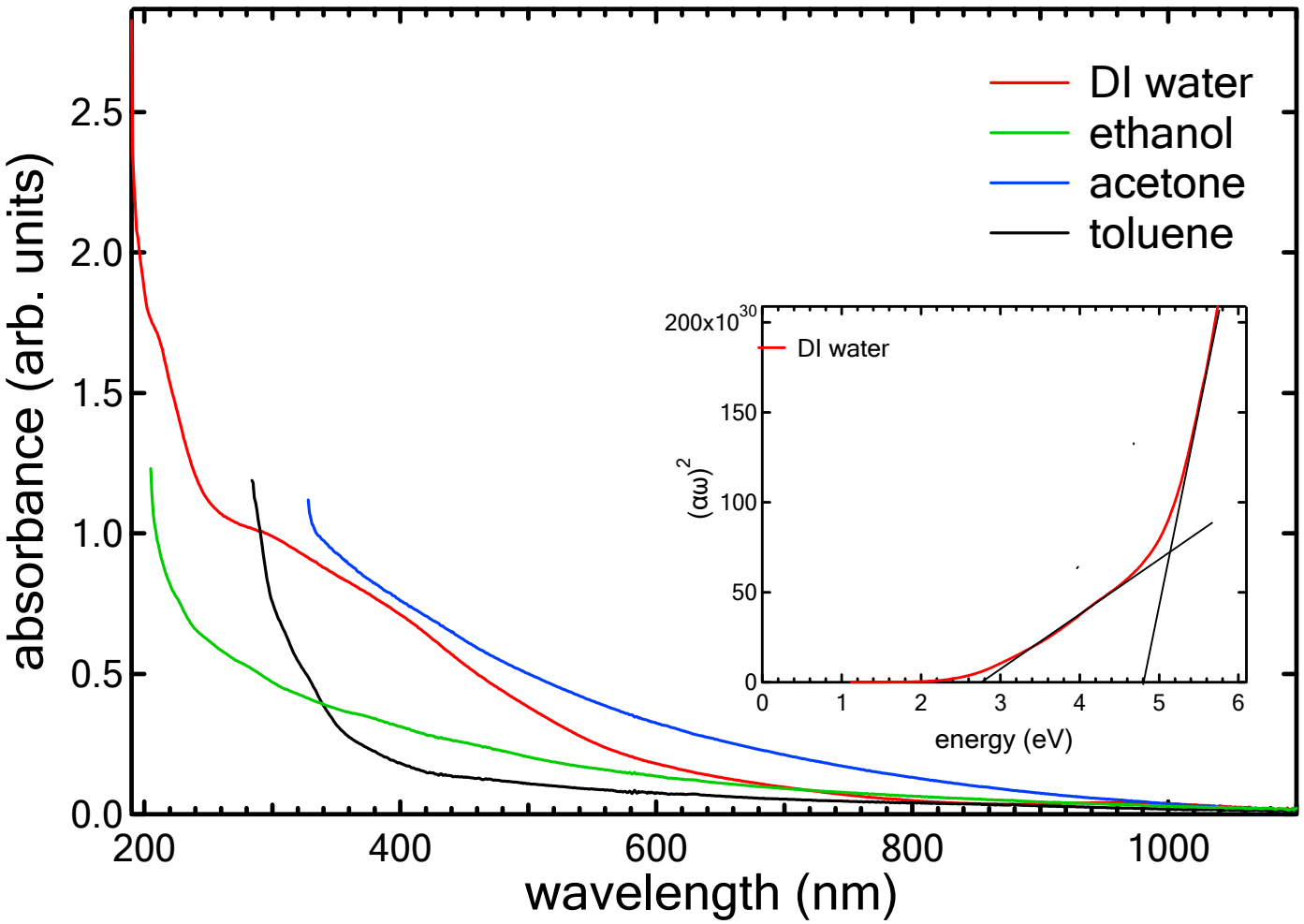
DI water
ethanol
acetone
toluene
absorbance (arb. units)
wavelength (nm)
0.0
0.5
1.0
1.5
2.0
2.5
200
400
600
800
1000
200x10^30
DI water
(αω)^2
150
100
50
0
0
1
2
3
4
5
6
energy (eV)

Fig. 3

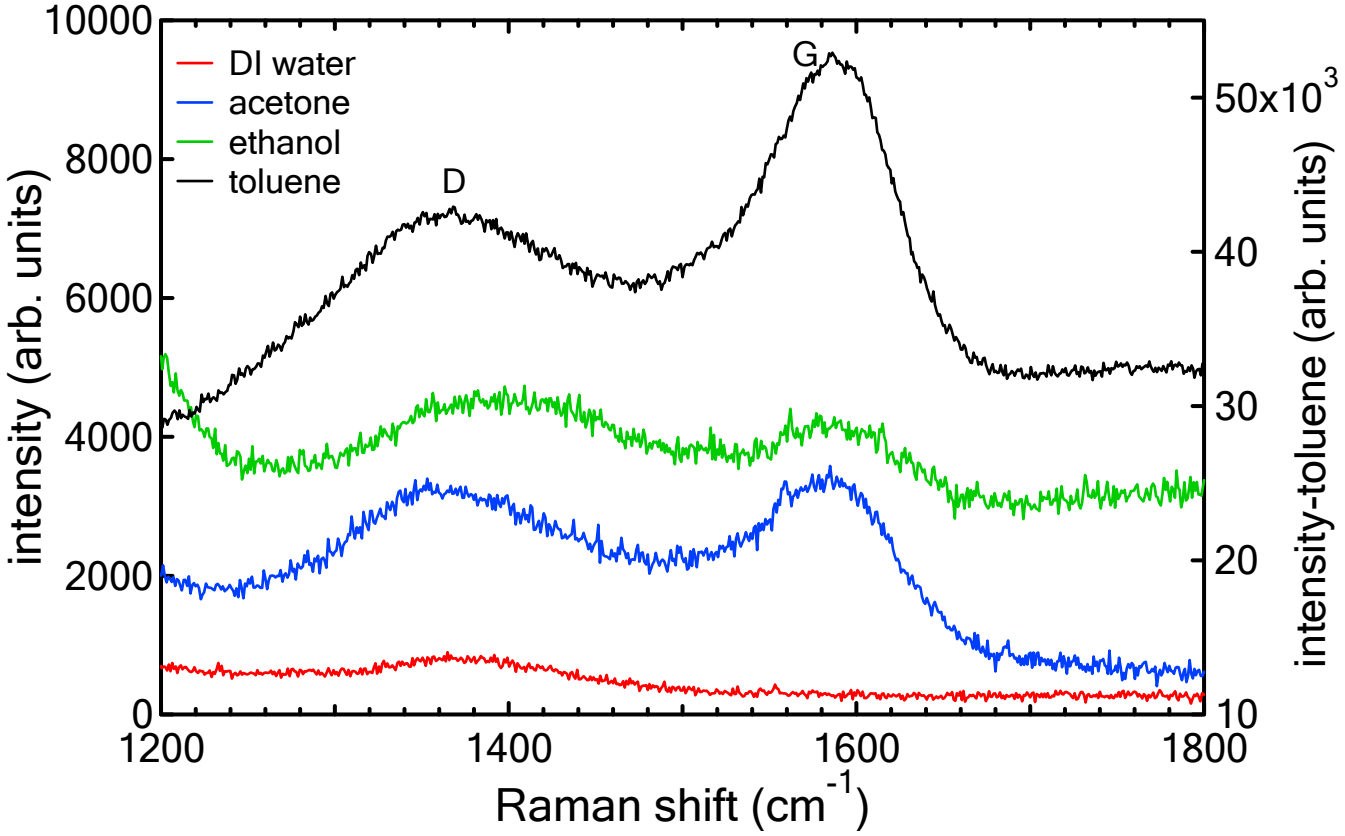
DI water
acetone
ethanol
toluene
D
G
intensity (arb. units)
intensity-toluene (arb. units)
Raman shift (cm-1)
10000
8000
6000
4000
2000
0
50x10^3
40
30
20
10
1200
1400
1600
1800

Fig. 4(a)

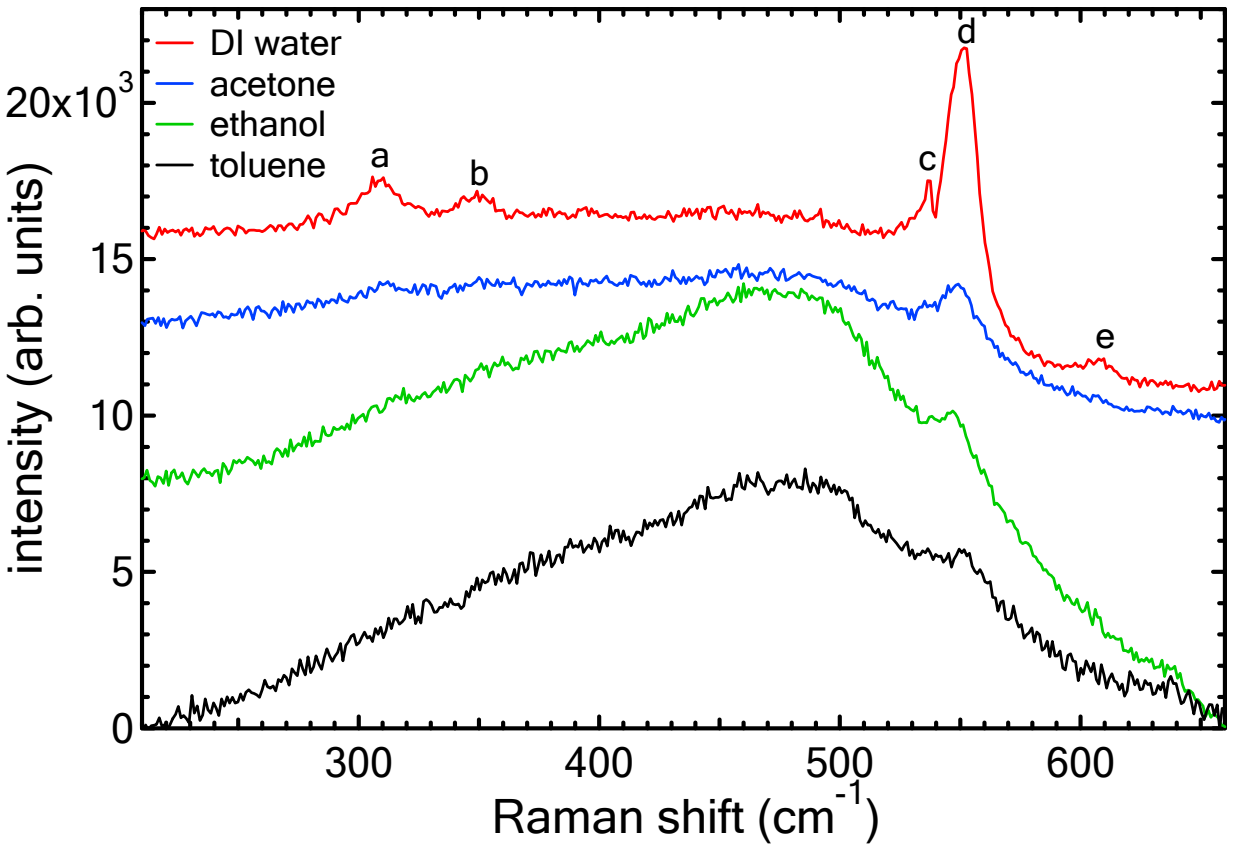
DI water
acetone
ethanol
toluene
a
b
c
d
e
20x10^3
15
10
5
0
intensity (arb. units)
300
400
500
600
Raman shift (cm^-1)

Fig. 4(b)